Two lanthanides in a macrocyclic ligand : consequences for the design of MRI contrast agents

a **spectroscopic** study

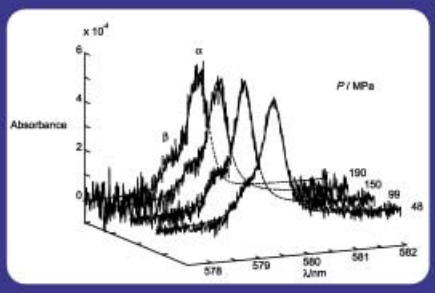

NMR
UV-visible
luminescence
EPR
^{1}H NMRD

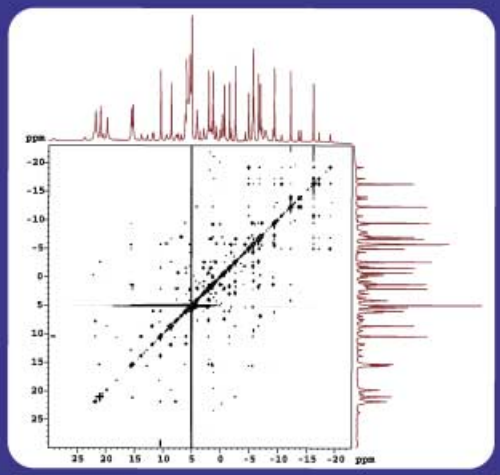

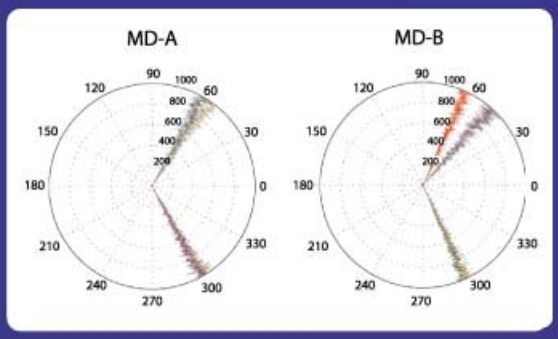

... and also a classical **molecular dynamics** study.

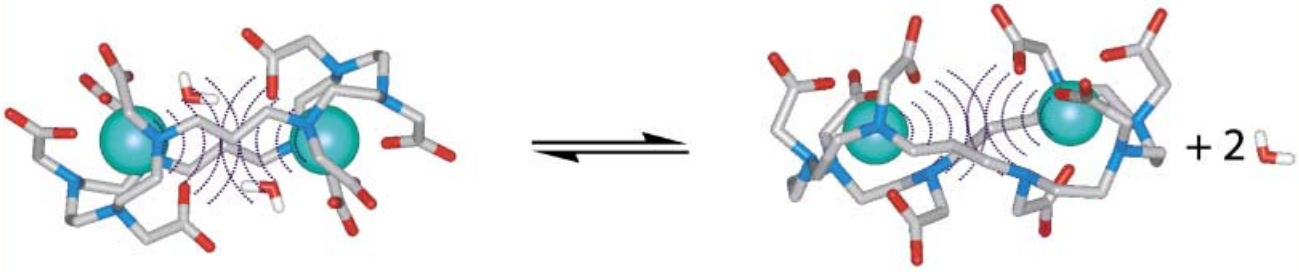

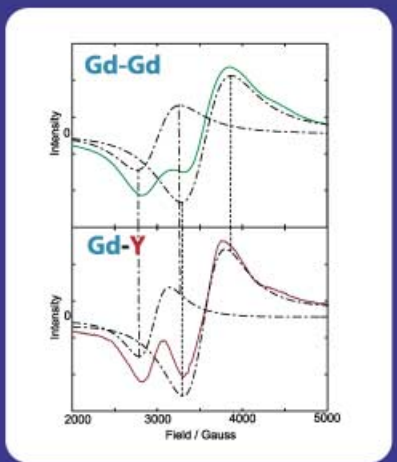

Intramolecular electronic interaction between the two close Gd^{III} increases the electronic relaxation rate.

For more details see the following pages.

 DOI: 10.1002/chem.200305049

Towards Binuclear Polyaminocarboxylate MRI Contrast Agents? Spectroscopic and MD Study of the Peculiar Aqueous Behavior of the Ln^{III} Chelates of OHEC (Ln = Eu, Gd, and Tb): Implications for Relaxivity

Gaëlle M. Nicolle,[a] Fabrice Yerly,[a] Daniel Imbert,[b] Ulrike Böttger,[c] Jean-Claude Bünzli,[b] and André E. Merbach*[a]

Abstract: We report the study of binuclear Ln^{III} chelates of OHEC (OHEC = octaazacyclohexacosane-1,4,7,10,14,17,20,23-octaacetate). The interconversion between two isomeric forms, which occurs in aqueous solution, has been studied by NMR, UV/Vis, EPR, and luminescence spectroscopy, as well as by classical molecular dynamics (MD) simulations. For the first time we have characterized an isomerization equilibrium for a Ln^{III} polyaminocarboxylate complex (Ln^{III} = Y, Eu, Gd and Tb) in which the metal centre changes its coordination number from nine to eight, such that: $[Ln_2(ohec)(H_2O)_2]^{2-} \rightleftarrows [Ln_2(ohec)]^{2-} + 2\,H_2O$. The variable temperature and pressure NMR measurements conducted on this isomerization reaction give the following thermodynamic parameters for Eu^{III}: $K^{298} = 0.42 \pm 0.01$, $\Delta H^0 = +4.0 \pm 0.2\ kJ\,mol^{-1}$, $\Delta S^0 = +6.1 \pm 0.5\ J\,K^{-1}\,mol^{-1}$ and $\Delta V^0 = +3.2 \pm 0.2\ cm^3\,mol^{-1}$. The isomerization is slow and the corresponding kinetic parameters obtained by NMR spectroscopy are: $k_{is}^{298} = 73.0 \pm 0.5\ s^{-1}$, $\Delta H_{is}^{\neq} = 75.3 \pm 1.9\ kJ\,mol^{-1}$, $\Delta S_{is}^{\neq} = +43.1 \pm 5.8\ J\,K^{-1}\,mol^{-1}$ and $\Delta V_{is}^{\neq} = +7.9 \pm 0.7\ cm^3\,mol^{-1}$. Variable temperature and pressure ^{17}O NMR studies have shown that water exchange in $[Gd_2(ohec)(H_2O)_2]^{2-}$ is slow, $k_{ex}^{298} = (0.40 \pm 0.02) \times 10^6\ s^{-1}$, and that it proceeds through a dissociative interchange I_d mechanism, $\Delta V^{\neq} = +7.3 \pm 0.3\ cm^3\,mol^{-1}$. The anisotropy of this oblong binuclear complex has been highlighted by MD simulation calculations of different rotational correlation times. The rotational correlation time directed on the Gd–Gd axis is 24% longer than those based on the axes orthogonal to the Gd–Gd axis. The relaxivity of this binuclear complex has been found to be low, since 1) only $[Gd_2(ohec)(H_2O)_2]^{2-}$, which constitutes 70% of the binuclear complex, contributes to the inner-sphere relaxivity and 2) the anisotropy of the complex prevents water molecules from having complete access to both Gd^{III} cages; this decreases the outer-sphere relaxivity. Moreover, EPR measurements for the Gd^{III} and for the mixed Gd^{III}/Y^{III} binuclear complexes have clearly shown that the two Gd^{III} centres interact intramolecularly; this enhances the electronic relaxation of the Gd^{III} electron spins.

Keywords: electronic relaxation · gadolinium · imaging agents · metal–metal interactions · MRI contrast agents

Introduction

Since the start of the magnetic resonance imaging (MRI) contrast agents' story about twenty years ago, many efforts have been made to directly correlate the structure of Gd^{III} chelates to the parameters that effect the efficiency of the potential drug in terms of imaging, that is, the so-called relaxivity, r_1.[1] In order to enhance r_1, it has been found that: 1) tumbling has to be slowed down by attaching the chelate to macromolecular assemblies, such as proteins,[2,3] dendrimers,[4,5] micellar aggregates[6,7] or polymers;[8] 2) the water-exchange rate has to be increased by promotion of the departure of a coordinated water molecule; this is achieved by the design of optimized chelates such as Gd^{III} complexes of TRITA (1,4,7,10-tetraazacyclotridecane-1,4,7,10-tetraacetic acid),[9] EPTPA (ethylenepropylenetriaminepentaacetic

[a] Prof. A. E. Merbach, G. M. Nicolle, F. Yerly
Laboratory of Inorganic and Bioinorganic Chemistry Institute of Molecular and Biological Chemistry
Swiss Federal Institute of Technology
EPFL-BCH, 1015 Lausanne (Switzerland)
Fax: (+41) 21-693-98-75
E-mail: andre.merbach@epfl.ch

[b] Dr. D. Imbert, Prof. J.-C. Bünzli
Laboratory of Lanthanide Supramolecular Chemistry
Institute of Molecular and Biological Chemistry
Swiss Federal Institute of Technology
EPFL-BCH, 1015 Lausanne (Switzerland)

[c] Dr. U. Böttger
Institute of Chemistry, Humboldt University
Brook-Taylor-Str. 2, 12489 Berlin (Germany)

Supporting information for this article is available on the WWW under http://www.chemeurj.org or from the author.

DOI: 10.1002/chem.200305049

acid)[10] or HOPO (hydroxypyridinonate) derivatives;[11,12] and 3) the hydration number can be increased, as in the case of TTAHA (triethylenetetramine-1,1,4,7,10,10-hexaacetic acid) chelates[13] or HOPO derivatives. These three parameters are of prime importance for the inner-sphere contribution to relaxivity. A fourth parameter, which is the electronic relaxation of the electron spin of Gd^{III}, is missing from this list. This term affects both inner- and outer-sphere relaxivities. It becomes particularly critical for macromolecular Gd^{III} complexes that have high water-exchange rates, and which are now at the centre of discussion. For such systems, any additional contribution to the electronic relaxation will prevent the increase of r_1.[1] Unfortunately, for a given coordination number, very little is known about the relationship between the structure of the complex and the electronic behaviour of the metal. In this paper we address this problem, and attempt to answer the question: does the proximity of the Gd^{III} cations affect the electronic relaxation?

A few years ago, a solution study of a trinuclear Gd^{III}–TACI (1,3,5-triamino-1,3,5-trideoxy-*cis*-inositol) complex indicated that the transverse electronic relaxation rate for the Gd^{III} electron spins increased as the distance between the paramagnetic centers ($r_{Gd-Gd} = 3.7$ Å) decreased.[14] The influence on the proton relaxivity was discussed. Unfortunately, this chelate is not typical of the polyaminocarboxylate Gd^{III} chelates that are currently used as contrast agents. A better model, namely the binuclear Gd^{III} chelate of the OHEC ligand (OHEC = octaazacyclohexacosane-1,4,7,10,14,17,20,23-octaacetate),[15,16] which is depicted in Figure 1, was investigated in the present study. In this binuclear complex the paramagnetic ions are about 6.5 Å apart.[17] For a mononuclear complex, concentrations higher than 5 M would ensure such short intermolecular distances. If the complex is soluble to such an extent, a concentration effect on the transverse electronic relaxation rate as described by an intermolecular contribution to the electronic relaxation[18] would probably exist even at MRI fields. Therefore, the influence of the intramolecular proximity has to be verified for this particular system. Furthermore, a ^1H NMR study on the diamagnetic binuclear Y^{III} complex of OHEC in solution showed the presence of two isomers.[17]

Before any relaxation study is begun, the thermodynamics and kinetics of the isomerization have to be clarified. As a result, high-resolution luminescence, NMR, UV/Vis, and EPR experiments have been performed. These studies, along with a classical molecular dynamic (MD) study of the complex allowed the two isomers to be characterised. The relaxation features of both binuclear Gd^{III} isomers have then been addressed by using ^{17}O NMR spectroscopy, ^1H relaxivity and EPR spectroscopy. Finally, the effect that proximity of the metal centers has on the electronic relaxation has been investigated by comparing the electronic relaxation of the Gd^{III} and mixed Gd^{III}/Y^{III} binuclear complex, in which one Gd^{III} ion has been replaced by the diamagnetic Y^{III} ion.

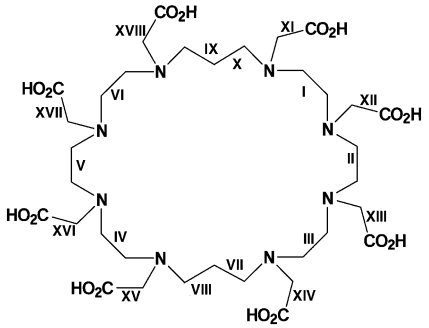

Figure 1. Chemical structure of the H_8OHEC (octaazacyclohexacosane-1,4,7,10,14,17,20,23-octaacetatic acid) ligand. The notations I to XVIII indicate the convention used for the dihedral angles on the ethylene and propylene bridges, NCCN and NCCC, respectively, and on the acetate arms NCCOB (OB = bound oxygen).

Results

High-resolution ^1H NMR study of the binuclear Eu^{III} complex of OHEC: The ^1H 1D-NMR spectrum at 274.8 K, which is depicted in Figure 2, shows two sets of relatively sharp signals; this is characteristic of two isomeric species that are undergoing slow exchange. The major isomer will be named α, and the minor one β. For the more populated isomer, 26 well-resolved peaks appear at low temperature; this is consistent with the centrosymmetry observed for the complex in the solid state.[17] The second set, which has at least 34 perceptible peaks, is not as well resolved, since some of the peaks overlap with the first more intense set. For the α isomer, one ^1H NMR peak corresponds to two protons, whereas for β, each peak corresponds to one proton. To assign the spectra, 2D-NMR experiments were carried out (see Supporting Information). The protons of the binuclear complex can be classified into three groups; the first two consist of the ethylene and propylene protons

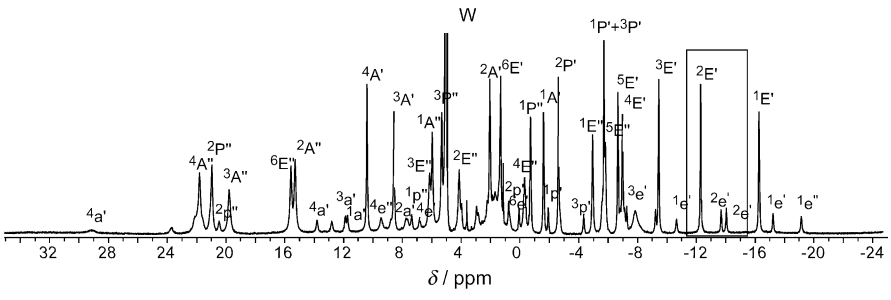

Figure 2. ^1H NMR spectrum of the binuclear Eu^{III} complex of OHEC at 600 MHz and 274.8 K. Notation for the major isomer, $[Eu_2(ohec)(H_2O)_2]^{2-}$ (α): acetate protons, from $^1A'$ to $^4A''$; propylene protons, from $^1P'$ to $^3P''$; and ethylene protons, from $^1E'$ to $^6E''$. ′ and ″ have been added to distinguish two geminal protons. For the minor isomer, $[Eu_2(ohec)]^{2-}$ (β), the same convention has been applied, and the protons from the α isomer (one signal) that exchange with protons from the β isomer (two signals as a result of lower symmetry) have been labelled with the equivalent lower-case letters. The labelled region has been used for the kinetic study. W = water protons.

of the carbon backbone, and the third corresponds to the protons of the acetate arms. A 400 MHz ^{1}H COSY45 spectrum allowed assignment of those protons that belong to the same fragment. To discriminate between J^2_{HH}-coupling and J^n_{HH}-coupling ($n>2$), a 400 MHz ^{13}C HMQC spectrum was recorded at low temperature (268.2 K). This enabled assignment of the protons directly bound to the same carbon. The COSY45 could not unambiguously distinguish between the ethylene and the propylene protons, so a 600 MHz ^{1}H TOCSY spectrum was recorded; this allowed the two types of protons to be differentiated. To avoid both overheating the sample and the ROE effect, a Clean-TOCSY sequence was chosen. These three 2D spectra gave crosspeaks that corresponded principally to the α isomer, for which the peaks are more intense. To assign the peaks of the β isomer, a ^{1}H NOESY spectrum was also recorded at 600 MHz. Pure exchange spectroscopy (EXSY) cross peaks between the peaks characterized for the α isomer and the nondefined peaks of the β isomer allowed assignment of the latter; this is depicted in Figure 2. Most of the ethylene protons for both the major and the minor isomer appear upfield of the free water protons. The propylene protons, except for ^{2}P″, are almost as shielded as the water protons, whereas the majority of the acetate protons are deshielded. The shielding that the different proton types of the binuclear Eu^{III} complex of OHEC display is significantly different to that shown by the Eu^{III} complexes of DOTA (1,4,7,10-tetra(carboxymethyl)-1,4,7,10-tetraazacyclododecane), DTPA (1,1,4,7,7-diethylenetriaminepentaacetic acid) or DTPA-dien (1,4,7-tris(carboxymethyl)-9,17-dioxo-1,4,7,10,13,16-hexaazacyclooctadecane).[19–21] The proton chemical shifts for the DOTA and DTPA complexes are in agreement with the proposed angular dependence of the pseudo-contact shift for these axially symmetric systems. Unfortunately, in this study such considerations cannot be made due to the lower symmetry of the binuclear chelate. The differences observed in the chemical shifts may indicate that the electron density around the metal and, therefore, the magnetic axis, is not comparable with the common DOTA or DTPA complexes. This could be due to the presence of the second metal center.

Kinetics and thermodynamics for the isomerization of the binuclear Eu^{III} complex of OHEC: The thermodynamics and kinetics for the isomerization were studied at pH 8.5 as a function of temperature and pressure by ^{1}H NMR spectroscopy between −25 and 32 ppm. The isomerization was found to be reversible with respect to pressure and temperature. The variable temperature and pressure ^{1}H NMR spectra (between 274.8 and 342.9 K, and from 0–200 MPa at 279.4 K; see Supporting Information) reveal that a chemical exchange occurs between two species: the line widths increase with temperature before they coalescence. As the complex decomposes at temperatures higher than 350 K, the temperature range used did not allow sharp coalesced peaks to be observed.

The isomerization rate constant k_{is}, which is defined as $\alpha \underset{}{\overset{k_{is}}{\rightleftharpoons}} \beta$, has been studied on the labelled region of the spectrum given in Figure 2, and has been enlarged as a function of temperature and pressure in Figures 3 and 4, respectively.

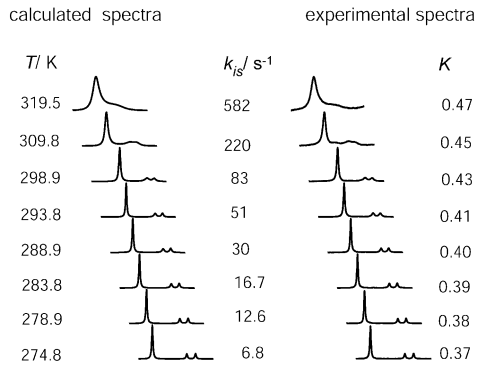

Figure 3. Temperature dependence of the isomerization rate constant, k_{is}, and of the equilibrium constant, $K=[\beta]/[\alpha]$, for the interconversion between $[Eu_2(ohec)(H_2O)_2]^{2-}$ (α) and $[Eu_2(ohec)]^{2-}$ (β), as studied by ^{1}H NMR spectroscopy at 600 MHz.

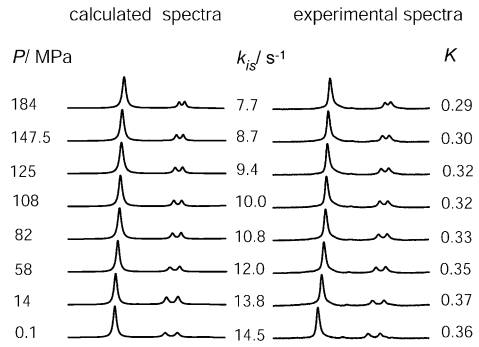

Figure 4. Pressure dependence of the isomerization rate constant, k_{is}, and of the equilibrium constant, $K=[\beta]/[\alpha]$, for the interconversion between $[Eu_2(ohec)(H_2O)_2]^{2-}$ (α) and $[Eu_2(ohec)]^{2-}$ (β), as studied by ^{1}H NMR spectroscopy at 400 MHz and at 279.4 K.

In these spectra the ^{2}E′ protons (two protons) of the major α isomer exchange with two protons, both named ^{2}e′, of the minor β isomer. The inverse of the mean lifetime of the α isomer, $\frac{1}{\tau_\alpha}=k_{is}$, was extracted from the ^{1}H NMR spectra by line shape analysis using Kubo–Sack formalism and the 3×3 exchange matrix D [Eq. (1)].[22,23]

$$D=\begin{bmatrix} -k_{is} & \frac{k_{is}}{2} & \frac{k_{is}}{2} \\ \frac{P_{E'}}{2P_{e'}}k_{is} & -\frac{P_{E'}}{2P_{e'}}k_{is} & 0 \\ \frac{P_{E'}}{2P_{e'}}k_{is} & 0 & -\frac{P_{E'}}{2P_{e'}}k_{is} \end{bmatrix} \quad (1)$$

D is composed of one site from the major α isomer, $^1H_{2E'}$, and of two sites from the minor one, $^1H_{2e'}$. For the calculation of each spectrum presented in Figures 3 and 4, the population of the two peaks of β ($P(^1H_{2e'})=P_{e'}$) has been taken to be equal. The line width in the absence of exchange has been extrapolated from the fitting of the line widths at lower temperature and pressure. The kinetic rate constant is assumed to obey Eyring law [Eq. (2)] in which k_{is}^{298} is the kinetic constant for isomerization at 298.15 K, and $\Delta H_{is}^{\pm}$ and $\Delta S_{is}^{\pm}$ are the activation enthalpy and entropy for the isomerization, respectively. R is the universal gas constant.

$$\frac{1}{\tau_\alpha} = k_{is} = \frac{k_B T}{h}\exp\left\{\frac{\Delta S^{\ddagger}_{is}}{R} - \frac{\Delta H^{\ddagger}_{is}}{RT}\right\} = \frac{k^{298}_{is} T}{298.15}\exp\left\{\frac{\Delta H^{\ddagger}_{is}}{R}\left(\frac{1}{298.15} - \frac{1}{T}\right)\right\} \quad (2)$$

The high-pressure measurements were conducted at low temperature (279.4 K) to ensure that a good resolution was obtained between the three signals, $^2E'$ and $2\times{}^2e'$. The effect of pressure on the ^1H NMR spectra is presented in Figure 4. The isomerization rate constant is assumed to have a pressure dependence in accord with Equation (3), in which $\Delta V^{\ddagger}_{is}$ is the activation volume and k^0_{is} is the isomerization rate constant at 279.4 K and zero pressure.

$$\ln(k_{is}) = \ln(k^0_{is}) - \frac{\Delta V^{\ddagger}_{is}}{RT}P \quad (3)$$

The simulated variable temperature and pressure spectra are presented in Figures 3 and 4, respectively, and lead to the following parameters: $k^{298}_{is} = 73.0 \pm 0.5\ s^{-1}$, $\Delta H^{\ddagger}_{is} = 75.3 \pm 1.9\ kJ\,mol^{-1}$, $\Delta S^{\ddagger}_{is} = 43.1 \pm 5.8\ J\,K^{-1}\,mol^{-1}$, $k^0_{is} = 14.4 \pm 0.4\ s^{-1}$ (at 279.4 K) and $\Delta V^{\ddagger}_{is} = 7.9 \pm 0.7\ cm^3\,mol^{-1}$.

The isomerization equilibrium constant K was calculated for the formation of the minor β isomer, that is for $\alpha \overset{K}{\Leftrightarrow} \beta$, and was also deduced from population ratios of previous spectral analyses such that $K = 2\times p(^1H_{2e'})/p(^1H_{2E'})$. We made the assumption that the temperature dependence of the isomerization equilibrium constant followed the simple Arrhenius law expressed in Equation (4) in which K^{298} is the equilibrium constant at 298.15 K, and ΔH^0 and ΔS^0 are the standard enthalpy and entropy for the isomerization, respectively.

$$K = K^{298}\exp\left\{\frac{-\Delta H^0}{R}\left(\frac{1}{T} - \frac{1}{298}\right)\right\} = \exp\left\{\frac{-\Delta H^0}{RT} + \frac{\Delta S^0}{R}\right\} \quad (4)$$

The logarithm of K versus pressure measured at 279.4 K was taken to be proportional to the standard reaction volume of isomerization, ΔV^0, as expressed in Equation (5) in which K_0 and K_P are the equilibrium constants at temperature T, and at zero and P pressure, respectively.

$$\ln(K_P) = \ln(K_0) - \frac{\Delta V^0}{RT}P \quad (5)$$

The thermodynamic parameters obtained are: $K^{298} = 0.42 \pm 0.01$, $\Delta H^0 = +4.0 \pm 0.2\ kJ\,mol^{-1}$, $\Delta S^0 = +6.1 \pm 0.5\ J\,K^{-1}\,mol^{-1}$, $K_0 = 0.37 \pm 0.01$ (at 279.4 K) and $\Delta V^0 = +3.2 \pm 0.2\ cm^3\,mol^{-1}$.

The UV/Vis spectra of the binuclear Eu^{III} chelate of OHEC were recorded between 577.5 and 581.5 nm at variable temperature and pressure. This spectral range corresponds to the $^7F_0 \rightarrow {}^5D_0$ transition, which is known to be sensitive to the Eu^{III} environment and particularly to its coordination number.[1,24] Two species are clearly present in the spectra presented in Figures 5 and 6; one minor species at about 579.3 nm and one major species at lower energy (ca. 579.7 nm). Each transition was described with a Gaussian–Lorentzian convolution. The equilibrium constant K was calculated from the population ratio between the minor and the major species. Equations (4) and (5) were used to take into account temperature and pressure dependence, respectively. The two species were assumed to have the same molar absorption coefficient; this implies that the integral ratio for each transition is equal to the population ratio. The thermodynamic parameters K^{298}, ΔH^0 and ΔS^0 were obtained from the simultaneous fit of the variable temperature spectra (Figure 5), and ΔV^0 was obtained from the simultaneous fit of the variable pressure spectra (Figure 6). The results are given in Table 1.

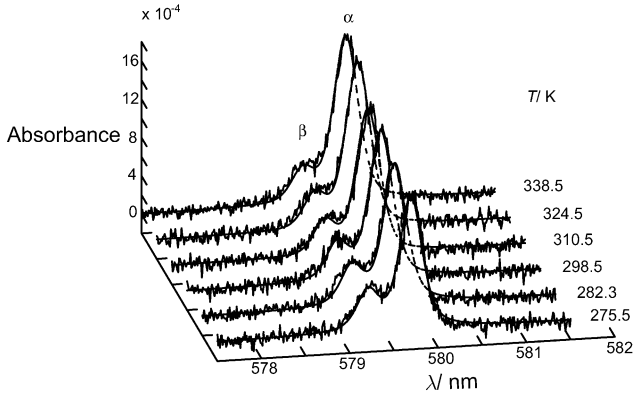

Figure 5. Temperature dependence of the $^7F_0 \rightarrow {}^5D_0$ transition in the UV/Vis spectra of the binuclear Eu^{III} chelate of OHEC ($C_{Eu^{III}}$ about 30 mmol kg^{-1}).

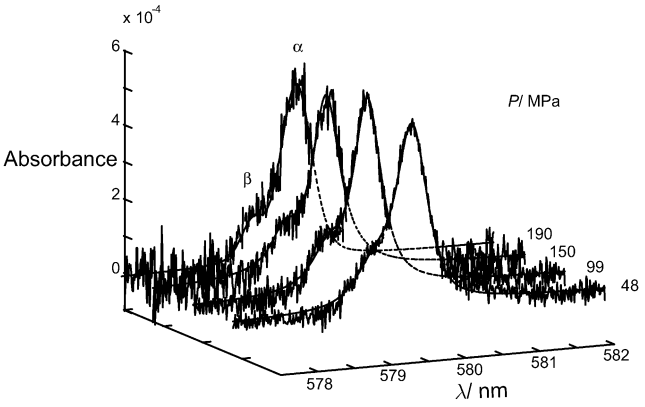

Figure 6. Pressure dependence at 298.2 K of the $^7F_0 \rightarrow {}^5D_0$ transition in the UV/Vis spectra of the binuclear Eu^{III} chelate of OHEC ($C_{Eu^{III}}$ about 10 mmol kg^{-1}).

Table 1. Thermodynamic parameters for the equilibrium between $[Ln_2(ohec)(H_2O)_2]^{2-}$ and $[Ln_2(ohec)]^{2-}$ (α and β isomers, respectively) obtained from the fit of the ^1H NMR and UV/Vis data on the Eu^{III} complex and EPR data on the Gd^{III} complex.[a]

	$K^{298} = [\beta]/[\alpha]$	ΔH^0 [kJ mol^{-1}]	ΔS^0 [J K^{-1} mol^{-1}]	ΔV^0 [cm^3 mol^{-1}]
^1H NMR	0.42 ± 0.01	$+4.0 \pm 0.2$	$+6.1 \pm 0.5$	$+3.2 \pm 0.2$ (279.4 K)
UV/Vis	0.40 ± 0.02	$+3.8 \pm 0.1$	$+5.2 \pm 0.2$	$+5.7 \pm 1.2$ (298.2 K)
EPR	0.44 ± 0.04	$+4.0 \pm 0.1$	$+6.6 \pm 0.3$	–

[a] The temperature ranges for the determination of K were: a) 274.8–298.9 K (^1H NMR), b) 275.5–338.5 K (UV/Vis) and c) 273.9–342.7 K (EPR).

The EPR spectra show the presence of two species in equilibrium. Figure 7 presents the temperature dependence of the line width and the resonance frequency. The EPR signal of each species was fitted to a Lorentzian shape and was described with empirical parameters such as line widths,

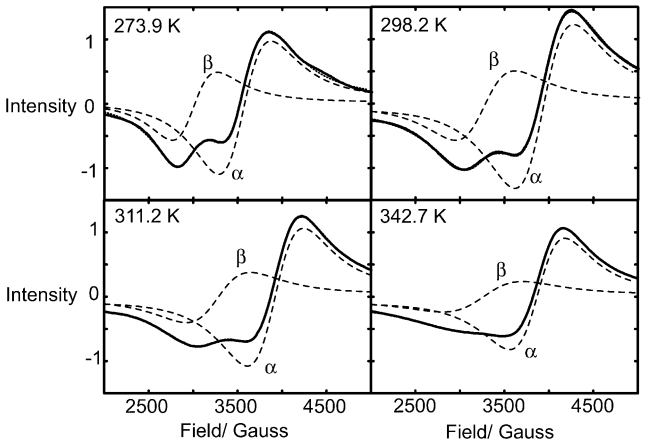

Figure 7. Temperature dependence of selected EPR spectra of the binuclear Gd^{III} chelate of OHEC and its isomers $[Gd_2(ohec)(H_2O)_2]^{2-}$ (α) and $[Gd_2(ohec)]^{2-}$ (β) at X-band (0.34 T). The dotted lines represent the calculated spectra for each isomer.

center fields, populations of each species and phasing parameters.[25] This enabled determination of the equilibrium constant [equal to the population ratio between the minor and the major species, Eq. (4)]. The thermodynamic parameters were also determined by using a simultaneous fit of the EPR spectra for seven different temperatures.

All thermodynamic parameters that were determined for the Eu^{III} chelate from ^1H NMR and UV/Vis spectroscopy, and for the Gd^{III} chelate from EPR spectroscopy, are given in Table 1. These values are equal within the experimental errors, although this is not necessary since two elements (Eu and Gd) have been chosen to calculate the equilibrium constant.

To see what effect ionic radius has on the equilibrium constant, the homobinuclear complex of the Tb^{III} ion, which is a neighbouring lanthanide to the Gd^{III} ion, was investigated. The spectra are presented in the Supporting Information. Unfortunately, the ^1H NMR signals were too broad to be integrated with high accuracy, especially for the minor isomer, and, therefore, an accurate equilibrium constant could not be determined. The thermodynamic parameters estimated for the binuclear Tb^{III} complex of OHEC were found to be very similar to those obtained for the Eu^{III} analogue, and are: $K^{298}=0.3\pm0.1$, $\Delta H^0=3.3\pm0.5\ kJ\,mol^{-1}$, and $\Delta S^0=+1\pm1\ J\,K^{-1}$.

Hydration number of the α and β isomers: At this stage, the presence of two isomers had been established and their macroscopic properties had been determined. A reasonable hypothesis is that the α and β isomers are in equilibrium: the major isomer α being $[Ln_2(ohec)(H_2O)_2]^{2-}$ and the minor isomer β being $[Ln_2(ohec)]^{2-}$ (Ln^{III} = Eu, Gd or Tb). The UV/Vis and EPR techniques, which are very sensitive to the inner coordination sphere of a metal, showed the existence of two distinct sites in solution. The difference of approximately 14 cm^{-1} between the two UV/Vis transitions can be accounted for by the nephelauxetic effect that arises as a result of the variation of one water molecule in the inner sphere of the Eu^{III} ion.[26] This is confirmed by the positive reaction volume obtained by UV/Vis ($\Delta V^0=+5.7\pm1.2$ $cm^3\,mol^{-1}$) and NMR spectroscopy ($\Delta V^0=+3.2\pm0.2$ $cm^3\,mol^{-1}$), indicating that β is the nonhydrated species. Moreover, the equilibrium constants ($K=[\beta]/[\alpha]$) reported in Table 1 have been calculated by assuming that within each α and β isomer there is either none or one water molecule per metal center (for the pair of complexes α:β it means 0:0, 0:2, 2:0, or 2:2 coordinated water molecules, respectively). If the β isomer actually had one coordinated water molecule (i.e., $[Ln_2(ohec)(H_2O)]^{2-}$), this would lead to the determination of different equilibrium constants for the binuclear Eu^{III} chelate of OHEC by UV/Vis and NMR spectroscopy. Assignment of the α and β isomers is also consistent with relaxometric data analysis, particularly with respect to the value obtained for the scalar coupling constant for α, $\frac{A}{\hbar}=-3.7\times10^6\ rad\,s^{-1}$. It should be noted that this value was obtained from the temperature dependence of the ^{17}O transverse relaxation rates ($1/T_2$), since the slow water exchange prevented its determination from the ^{17}O NMR chemical shifts. To ascertain the hydration numbers of α and β we used direct-method luminescence and lifetime determinations.

The emission spectra of the binuclear Eu^{III} complex of OHEC have been measured both in solution (D_2O and H_2O) and in the solid state on the recrystallized compound. They display the characteristic Eu($^5D_0\rightarrow{}^7F_j$) transitions as shown in Figure 8 and are dominated by the transitions to

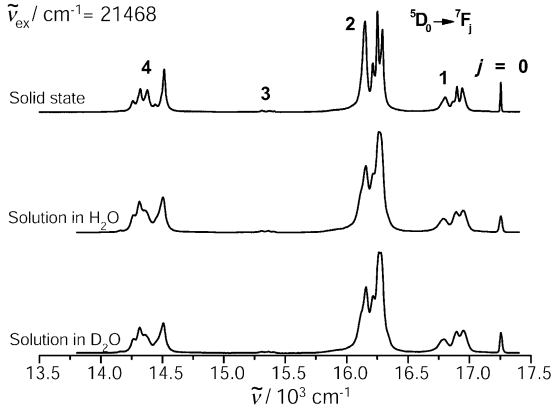

Figure 8. Emission spectra of the binuclear Eu^{III} chelate of OHEC in the solid state and in H_2O and D_2O at 295 K upon broad-band excitation ($^5D_2$) ($C_{Eu^{III}}=1.0\ mmol\,kg^{-1}$).

the $^7F_2$ sublevels. The relative corrected and integrated intensities of the $^5D_0\rightarrow{}^7F_j$ (j = 0–4) transitions, as well as the energy of the crystal-field sub-levels for the ^7F_j (j = 1–4) manifold (in water) are reported in the Supporting Information. The crystal-field splitting observed upon broad-band excitation ($^5D_2$) can be interpreted in terms of the existence of a low symmetry around the Eu^{III} ion, since the hypersen-

sitive transition $^5D_0 \rightarrow {}^7F_2$ exhibits at least four bands and a large intensity. The similar emission spectra obtained in both solution and the solid state indicate that the structure of the solid-state sample is maintained in solution. Moreover, when the solutions were diluted to 10^{-4} M the overall shape of the emission spectra was not affected. In the solid state, the strong $^5D_0 \rightarrow {}^7F_0$ transition, which is unique for a given chemical environment, displays a fairly symmetrical main band at 17256 cm^{-1} (full width at half height (fwhh) = 12 cm^{-1}) (lifetime analysis revealed a hydration number of one, as observed by X-ray spectroscopy).[17] In water, the excitation profile of the Eu($^5D_0 \rightarrow {}^7F_0$) transition, which was obtained by monitoring the most intense component of the $^5D_0 \rightarrow {}^7F_2$ transition (16273 cm^{-1}, Figure 9), displays bands

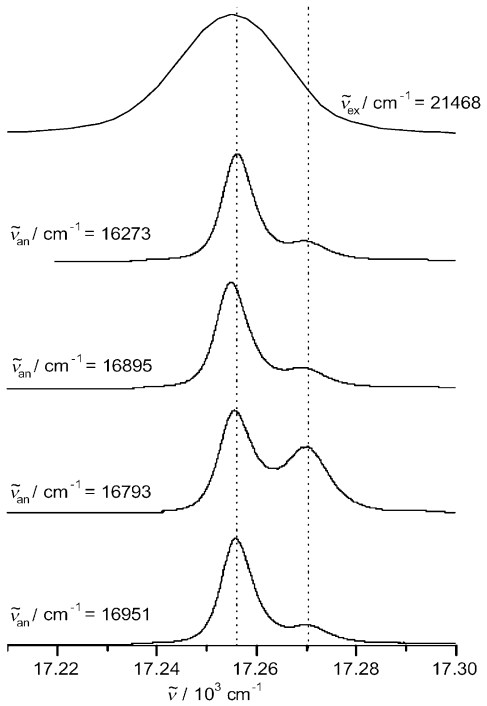

Figure 9. Excitation spectra at 295 K of the binuclear Eu^{III} chelate of OHEC in solution upon monitoring the Eu($^5D_0 \rightarrow {}^7F_{1,2}$) transitions and upon enlargement of the Eu($^5D_0 \rightarrow {}^7F_0$) transition [broad-band excitation ($^5D_2$)] ($C_{Eu^{III}} = 1.0$ mmol kg^{-1}).

that are analogous to those seen in the UV/Vis spectrum: a main band at 17256 cm^{-1} for the α isomer (symmetrical band, site α, fwhh = 9 cm^{-1}), and a weaker band at 17270 cm^{-1} (site β, fwhh = 11 cm^{-1}). When the components of the $^5D_0 \rightarrow {}^7F_1$ transition are monitored, bands α and β result. The experimental data once again demonstrate that the investigated compound contains two species: 1) β, which is strongly emitting and 2) α, which is weakly emitting and corresponds to another chemical environment. The excitation spectra in D_2O are identical with respect to the number of bands displayed and their intensities. Moreover, selective laser excitation of the two 0–0 transitions labelled α and β, both in H_2O and D_2O, produces two different emission spectra, both of which display the characteristics of the broad-band emission spectrum. The emission spectra at 10^{-4} M are similar. However, a population analysis of the $^5D_0 \rightarrow {}^7F_1$ transition recorded under broad-band excitation is difficult with the collected data because of a quasi-superimposition of the emission spectra that corresponds to all the species (broad-band excitation), as well as to the α isomer (excitation at 17255 cm^{-1}) (see Supporting Information). Nevertheless, a multi-peak fitting of the two high-resolution emission spectra in the $^5D_0 \rightarrow {}^7F_1$ region with excitation at 17255 and 17270 cm^{-1} allowed determination of the wavenumber and the full width at half height of the three maxima for each species. With these values, a multi-peak fitting of the emission spectrum upon broad-band ($^5D_2$) excitation enabled us to calculate that site β contributes 35 ± 9 % to the total emission to $^7F_1$; this is in agreement with the equilibrium constant determined previously in this study by other techniques. To access the metal hydration number for both isomers the emission lifetimes were measured in H_2O and D_2O. They are identical at 10^{-3} and 10^{-4} M, and were then used to calculate the number of coordinated water molecules per metal center q [Eqs. (6)–(8)] in which $k_{obs} = 1/\tau_{obs}$, $\Delta k_{obs} = k_{obs}(H_2O) - k_{obs}(D_2O)$, and k_{obs} is given in ms^{-1}.

$$q = 1.05(\Delta k_{obs}) \quad (6)$$

$$q = 1.2(\Delta k_{obs} - 0.25) \quad (7)$$

$$q = 1.11(\Delta k_{obs} - 0.31) \quad (8)$$

The luminescence decays of the $^5D_0$(Eu) excited state measured in water upon direct excitation are in the range 0.98–1.01 ms (site β, 17270–17275 cm^{-1}) and 0.55–0.57 ms (site α, 17249–17255 cm^{-1}). In constrast, luminescence decays measured in D_2O upon direct excitation are in the range 1.71–1.72 ms (site β, 17270—17275 cm^{-1}) and 1.62–1.65 ms (site α, 17249—17255 cm^{-1}). From Equation (6)[27], we obtained $q = 0.45$ and 1.25 for sites β and α, respectively. The estimated uncertainty for q is ±0.5. This early equation was established when crystallized complexes with $q = 1$–9 were used as references, in which interactions due to the molecules of water in the second coordination sphere were not taken into account. For Equation (7), which was proposed by Beeby et al. on the basis of measurements obtained for complexes in solution that had $q = 1$–3,[28] we obtained $q = 0.2$ and 1.15 for sites β and α, respectively. More recently, a refined equation [Eq.(8)][29] has been proposed for the Eu^{III} complexes in solution. It gives $q = 0.1$ and 0.95 for sites β and α, respectively. Therefore, Equations (7) and (8) give similar results, with an average of $q = 0.15$ and 1.05 for sites β and α, respectively, and an estimated uncertainly of ±0.1. Within experimental error, the α isomer can definitively be assigned to $[Eu_2(ohec)(H_2O)_2]^{2-}$ ($q = 1$), while the β isomer corresponds to $[Eu_2(ohec)]^{2-}$ ($q = 0$).

After the number of coordinated water molecules around the Eu^{III} ion in the binuclear complex was determined, it was also necessary to conduct a pH study into the potential deprotonation of the system. A pH dependence was not detected in the chemical shifts of the ^1H NMR spectra of the Eu^{III} complex (Supporting Information) between pH 8.7 and 11.4; this shows that the two species do not correspond to differently protonated ligands. Therefore, the observed temperature effect is not due to the temperature de-

pendence of a protonation constant. Moreover, the relaxivity (r_1) recorded at 30 MHz shows a plateau between pH 7.5 and 11. This means that there is no prototropic effect, which arises as a result of the deprotonation of water to give hydroxide, and consequently no increase in r_1 by fast proton exchange, which would give a more efficient propagation of the paramagnetic effect to bulk water.[30,31] Therefore, the presence of any coordinated hydroxide can be disregarded and the nature of the coordinated water molecule can be considered as H_2O at a pH of about nine.

Relaxivity of the binuclear Gd^{III} isomers of OHEC: ^{17}O NMR, EPR, and ^1H NMRD data have been fitted simultaneously according to the approach of Powell et al.[18] Spin rotation contributions of the electronic relaxation were not considered, but rotational correlation times for both the water protons [τ_R(H)] and the oxygen [τ_R(O)] were taken to be different.[32] In this particular case the mole fraction of coordinated water molecules (P_m) is related to the concentration of Gd^{III} ions in $[Gd_2(ohec)(H_2O)_2]^{2-}$. Hence, $P_m = C_{Gd}/(1+K)$ and is temperature dependent. The temperature dependence of K is described by the parameter obtained from the EPR study ($K^{298} = 0.44$ and $\Delta H^0 = 4.0\ kJ\,mol^{-1}$). By taking into account the relaxivity (r_1^α and r_1^β) contribution of each isomer as weighted by their mole fraction (x_α and x_β), the effective relaxivity can be derived from Equation (9) in which $x_\alpha = (1/1+K)$ and $x_\beta = 1-x_\alpha$.

$$r_1 = x_\alpha(r_{1is}^\alpha + r_{1os}^\alpha) + x_\beta r_{1os}^\beta \qquad (9)$$

The experimental data points and the corresponding fitted curves are shown in Figure 10. The temperature dependence of the ^{17}O transverse relaxation rates and chemical shifts is characteristic for a slow water exchange process. Indeed, the water-exchange rate determined is $(0.40 \pm 0.02) \times 10^6\ s^{-1}$. The variable pressure ^{17}O NMR study, which used the usual equation within the domain of slow exchange,[33] allowed the value of the activation volume $\Delta V^{\neq}$ to be determined using Equation 10 in which $\Delta V^{\neq}$ is the activation volume independent of pressure and $(k_{ex})_0^T$ is the water-exchange rate at zero pressure and temperature T.

$$\frac{1}{T_2} - \frac{1}{T_{2A}} \simeq P_m \times k_{ex} = \left(\frac{C_{Gd^{III}}}{1+K\exp\left\{-\frac{\Delta V^0}{RT}P\right\}} (k_{ex})_0^T \exp\left\{-\frac{\Delta V^{\neq}}{RT}P\right\} \right) \qquad (10)$$

A reasonable fit of the relaxivity profiles was obtained by fixing the distance of closest approach between the water molecule and the complex (a_{GdH}) to 4.5 Å. This is slightly higher than the value of 3.5 Å commonly used for small molecules with spherical geometry. It can be explained by the fact that the outer-sphere contribution was treated with the normal Freed's model,[34,35] in which the Gd^{III} complex is considered to be spherical; this is not the case in this study and will be discussed in the section that considers the anisotropy of the complex. The resulting parameters are presented in Table 2.

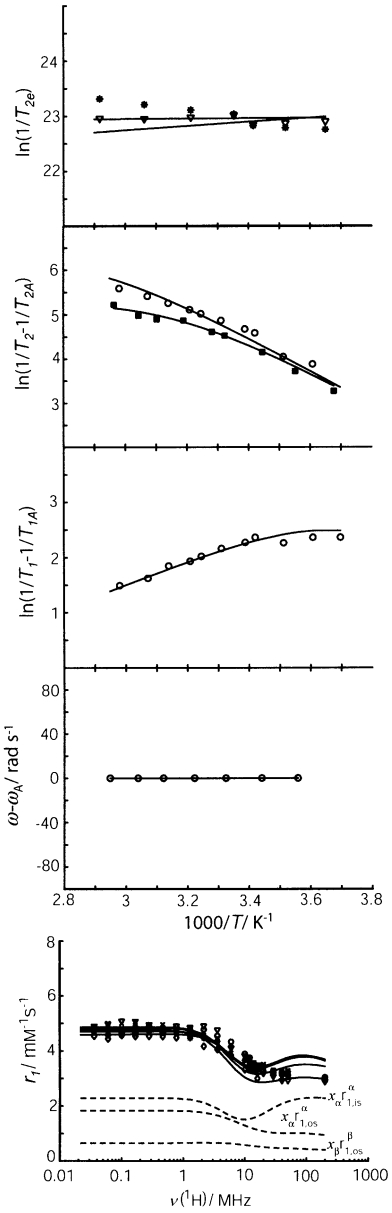

Figure 10. Temperature dependence, from the top, of the transverse electronic relaxation rate for the binuclear Gd^{III} isomers of OHEC: α (▽, bottom line) and β (*, top line); of ^{17}O transverse [at 9.4 T (○) and 4.7 T (■)] and longitudinal relaxation rates and chemical shifts at 9.4 T (○), respectively. Temperature dependence of the ^1H relaxivity profiles of the Gd^{III} complex of OHEC at 278.2 K (×), 288.2 K (◇), 298.2 K (*), 310.2 K (○), and 323.2 K (△). The dotted lines represent the calculated curves of each contribution to the relaxivity of α and β at 298.2 K.

The transverse electronic relaxation for the binuclear Gd^{III} complex of OHEC appears to be three times higher than for $[Gd(dota)(H_2O)]^-$. To highlight the proximity effect of the two Gd^{III} ions on the electronic relaxation, EPR spectra of the mixed diamagnetic/paramagnetic Y^{III}/Gd^{III} complex were recorded. The doping of the binuclear Y^{III} complex of OHEC with Gd^{III} ions was carried out in such a way that the contribution of the bis-Gd^{III} complex of OHEC could be neglected. The spectra presented in Figure 11 indicate the presence of two species, and are postulated to be the same type of isomers as in the homobinuclear

Table 2. Parameters obtained from the simultaneous fit of ^{17}O NMR, EPR, and ^{1}H NMRD data for the two isomers of the binuclear Gd^{III} complex of OHEC.[a,b]

	$[Gd_2(ohec)(H_2O)_2]^{2-}$		$[Gd_2(ohec)]^{2-}$
k_{ex}^{298} [10^6 s^{-1}]	0.40 ± 0.02		–
ΔH^{+} [$kJ\,mol^{-1}$]	30.9 ± 1.1		–
ΔS^{+} [$J\,mol^{-1}\,K^{-1}$]	-34 ± 3		–
ΔV^{+} [$cm^3\,mol^{-1}$]	$+7.3 \pm 0.3$		
$A/\hbar$ [10^6 $rad\,s^{-1}$]	-3.7 ± 0.3		–
C_{os}		*0*	
τ_R^{298}(O) [ps]	257 ± 20		–
E_R [$kJ\,mol^{-1}$]		17 ± 3	
τ_R(H)/τ_R(O)	0.81 ± 0.09		same τ_R(H)
τ_v^{298} [ps]	11 ± 1		25 ± 7
E_v [$kJ\,mol^{-1}$]	4.6 ± 1.6		*1*
Δ^2 [10^{20} s^{-2}]	0.92 ± 0.04		0.67 ± 0.05
r_{GdH} [Å]	*3.1*		
D_{GdH}^{298} [10^{-10} $m^2\,s^{-1}$]		23.2 ± 1.5	
E_{GdH} [$kJ\,mol^{-1}$]		*17*	
a_{GdH} [Å]		*4.5*	
$\chi(1+\eta^2/3)^{1/2}$ [MHz]	5.0 ± 0.8		
r_{GdO} [Å]	*2.5*		

[a] The italicized parameters were fixed for the fit. [b] For the temperature dependence of P_m the equilibrium constant for the reaction between $[Gd_2(ohec)(H_2O)_2]^{2-}$ and $[Gd_2(ohec)]^{2-}$ has been fixed to : $K^{298} = 0.44$ and $\Delta H^0 = 4.0\ kJ\,mol^{-1}$.

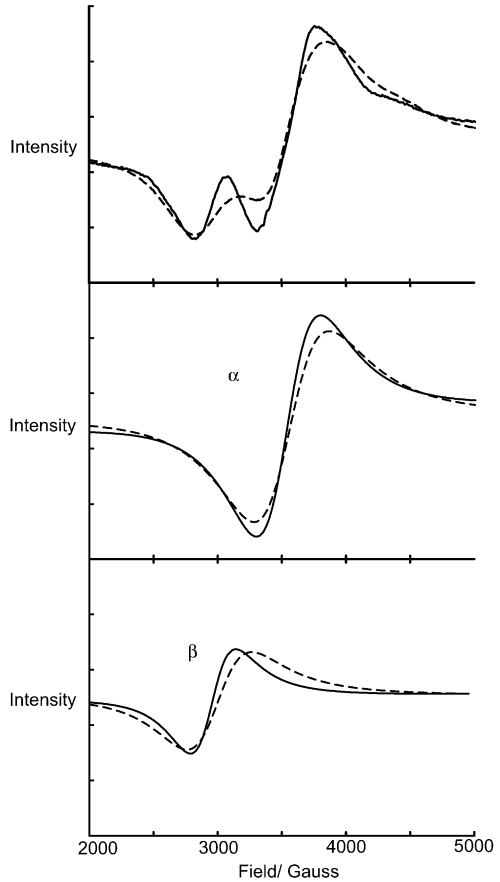

Figure 11. The effect on the EPR spectra of the α and β isomers at 273.9 K and at X-band upon replacing 90% of the Gd^{III} ions in the binuclear Gd^{III} chelate of OHEC with Y^{III} ions. The straight lines correspond to the mixed Gd^{III}/Y^{III} binuclear complex, while the dotted lines correspond to the bis-Gd^{III} complex. From the top global spectra, as well as the spectra for the α and β isomers, the following was determined: for the bis-Gd^{III}, $\Delta H_{pp,\alpha} = 582.5$ G and $\Delta H_{pp,\beta} = 502.1$ G; for the mixed Gd^{III}/Y^{III}, $\Delta H_{pp,\alpha} = 494.2$ G and $\Delta H_{pp,\beta} = 349.7$ G.

complex. Moreover, the equilibrium constant obtained for the formation of the minor isomer is very similar to that obtained in the homobinuclear case ($K^{298} = 0.31 \pm 0.04$; $\Delta H^0 = +4.4 \pm 0.2\ kJ\,mol^{-1}$). For any given temperature, the EPR peaks of the mixed Y^{III}/Gd^{III} complex were between 15 and 42% sharper (see Supporting Information); this implies that in the case of the bis-Gd^{III} chelate of OHEC, the transverse electronic relaxation rate is proportionally increased for both isomers.

Classical MD simulations: In order to perform a classical MD simulation of the α and β Gd^{III} isomers in solution, we started from the two X-ray structures available, namely $Na_2[Gd_2(ohec)(H_2O)_2]\cdot 12\,H_2O$ for MD-α, and $Na_2[Yb_2(ohec)]$ for MD-β.[17,36] Ligand conformational changes were not observed in either simulation; this indicates that both isomers are quite rigid. From the OHEC dihedral angle sequence defined in Figure 1, the α isomer has the *δλλλδδaaaa δλδδλδλλ* conformation and the β isomer has the *λδδλδδpapa δδλλδδλλ* conformation. The greek letters *δ* and *λ* refer to standard stereochemical labels, *p* means an eclipsed positive angle (about 150°), and *a* means an anti angle (180°). A table of the time averaged dihedral angles I to XVIII can be found in the Supporting Information. Water molecules do not leave or enter the Gd^{III} coordination polyhedron during both 1 ns simulations. Selected distances are reported in Table 3. Hydrogen bonds are observed between the inner-sphere water hydrogen atoms and an acetate oxygen atom (OB = bound oxygen) bound to the Gd^{III} ion. From time to time the two hydrogen atoms exchange their positions. We define the H–O distance as the closest distance between the water hydrogen and the OB. The position of the water molecule in the coordination polyhedron in MD-α was examined by applying the algorithm developed by Yerly et al.[37] It was found that the oxygen lies in the prismatic position of a monocapped square antiprism with C_{4v} symmetry. The capping position here, which is usually occupied by a water oxygen atom as in DOTA-like complexes, has an acetate oxygen atom (OB) instead. In MD-β, a distorted square antiprism was observed around both Gd^{III} ions. A representation of these structures is given in Figure 12. The angular projections of the coordination polyhedrons centered on the C_4 axis are available as Supporting Information.

Table 3. Selected time-averaged interatomic distances obtained from MD simulations.[a]

	Distance [Å]	
	MD-α	MD-β
Gd–N	2.64 (0.09)	2.57 (0.07)
Gd–OB	2.57 (0.24)	2.46 (0.06)
Gd–OWC	2.53 (0.07)	–
Gd–Gd	6.61 (0.11)	6.79 (0.13)
Gd–HWC	3.20 (0.20)	–
H···O	1.80 (0.17)	–

[a] Numbers in brackets correspond to one standard deviation. N = ligand nitrogen atoms, OB = ligand acetate oxygen atoms bound to the Gd^{III} ions, OWC = coordinated water oxygen, HWC = hydrogen of the coordinated water molecule, H···O is the distance between one proton of the coordinated water molecule and the closest acetate oxygen atom.

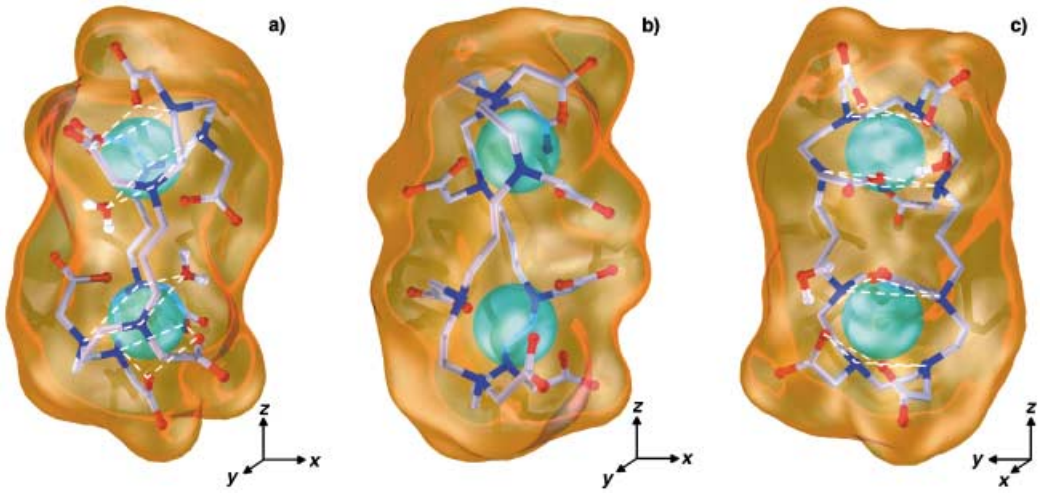

Figure 12. Molecular structures of the α and β isomers as determined by MD simulations and semi-transparent Connolly surfaces (blue = nitrogen, red = oxygen, grey = carbon, and white = hydrogen). Principal axes of both isomers are labelled *x, y,* and *z*: a) $[Gd_2(ohec)(H_2O)_2]^{2-}$ = α, b) $[Gd_2(ohec)]^{2-}$ = β and c) the β isomer with its two well-localized water molecules rotated by 90°. The dashed white lines, which link the Gd^{III} coordination sites, form two planes that are orthogonal to the C_4 axis [C_{4v} (α) and D_{4d} (β)].

A water molecule is not observed to leave or enter in either the MD-α or MD-β simulations. To begin with we removed the two coordinated water molecules from $[Gd_2(ohec)(H_2O)_2]^{2-}$ and performed an energy minimization of the complex in vacuo. The complex was then placed into a water bath and an MD simulation was started. Two water molecules immediately entered into the first coordination sphere of the Gd^{III} ion at the same positions found in the MD-α simulation.

To understand the water-exchange rate (k_{ex}) in Gd^{III} polyaminocarboxylates, we quantified the available space for a coordinated water molecule in the first coordination sphere by determining the solid angle, Ψ. This angle, which is centred on the Gd^{III} ion and is bordered by the neighbouring water oxygen coordination sites, is a possible descriptor for the steric constraint of the complex on the bound water molecule. When Ψ is large the complex can easily accept a water molecule, and a low water-exchange rate is implied. A decrease in Ψ increases the water-exchange rate until there is not enough space in the complex for a water molecule to sit in the inner sphere. The calculated Ψ around the water molecules in MD-α is 4.9 ± 0.3 steradian; this is larger than the value of 3.6 steradian obtained for $[Gd(egta)(H_2O)]^-$.[37]

From MD simulation trajectories it is possible to calculate the second-order rotational correlation time (τ_R) relevant for NMR spectroscopy. The τ_R value is extracted from the time evolution of a given vector.[38] This vector can be defined by two atoms, or groups of atoms, and enables the global molecular tumbling rate, as well as the local tumbling rate of one atom around the metal ion to be calculated. Table 4 gives the rotational correlation times calculated for various vectors.

To better understand the distribution of water molecules around the complex, radial distribution functions of the water oxygens and hydrogens, $g(r)$, have been calculated for three different centers, namely the two Gd^{III} ions and their barycentre. These centers were chosen so that the anisotropy of the complex as a result of its oblong shape would be taken into account. The $g(r)$ around the two Gd^{III} ions describes the hydration around the extremities of the complex, whereas $g(r)$ around the barycentre describes the hydration in the middle of the complex. In the MD simulations of the two isomers, the $g(r)$ values around the two Gd^{III} centres are not significantly different. For that reason we represented $g(r)$ only around one Gd^{III} ion of each isomer in Figure 13.

Table 4. Rotational correlation times calculated from MD-α and MD-β simulations.[a]

Time [ps]	MD-α	MD-β
$\tau_R(x)$	140	113
$\tau_R(y)$	166	152
$\tau_R(z)$	190	168
τ_R(Gd–OW)	152	–
τ_R(Gd–HW)	127	–

[a] *x, y* and *z* vectors are colinear to *x, y* and *z* axes defined on Figure 12.

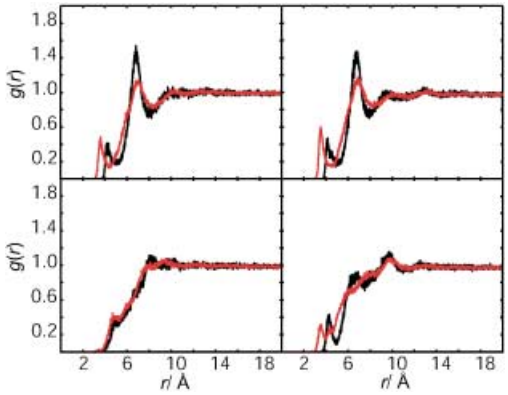

Figure 13. Radial distribution functions $g(r)$ of the water oxygen (black lines) and hydrogen (red lines) in MD-α (left side) and MD-β (right side). The top $g(r)$ have been calculated as having been centred on the Gd^{III} ions, whereas in the bottom graphs they have been centred on the corresponding barycentre.

The Gd^{III}–water oxygen radial distributions (Figure 13 top solid lines) show peaks at 4.22 (α) and 4.13 Å (β). Integration of these peaks indicates that 2.06 and 2.26 water molecules, respectively, are close to each Gd^{III} ion. The $g(r)$ for the water hydrogens shows peaks at 3.58 and 3.52 Å for the α and β isomers, respectively. Thus, there are two water molecules close to each Gd^{III} ion in both isomers, as a result of hydrogen bonds with the acetate oxygens. These water molecules have their hydrogen atoms pointing towards the lanthanide. It should be noted that the $g(r)$ values calculated for the barycentre are different for the two isomers. In MD-β, the two water molecules are well localized within the barycentre (between 3.8 and 4.9 Å from the barycentre, see Figure 13) as a result of hydrogen bonds with acetate oxygens in their vicinity. In MD-α the water molecules are not well localized and do not have a preferred orientation. In MD-β, as in the α isomer, there are four water molecules in close proximity to the complex. In the β isomer, two of the four water molecules are linked to acetates that are close to the barycentre (they appear in both $g(r)$ as being either centered on the Gd^{III} ion or on the barycentre). Figure 12c) illustrates the two sites occupied by these two water molecules. They lie on the same side of the yz plane, which separates the two inner-sphere coordinated water molecules (for comparison, the MD-α is shown in Figure 12a). It was possible to calculate the residence time of the confined water molecules in MD-β. For each site, ten water exchanges occur during a 1 ns simulation. This corresponds to a residence time ($t_{1/2}$) of about 100 ps.

The reaction volume (ΔV^0) for the reaction $\alpha \rightleftarrows \beta + 2H_2O$ is expressed as $\Delta V^0 = V^0(\beta) + 2V^0(H_2O) - V^0(\alpha)$. From the MD simulations, the following Connolly volumes have been calculated in solution: $V^0(\alpha) = 531 \pm 3\ cm^3 mol^{-1}$, $V^0(\beta) = 515 \pm 3\ cm^3 mol^{-1}$ and $V^0(\beta + 2H_2O) = 541 \pm 3\ cm^3 mol^{-1}$. The last volume corresponds to the β isomer in which the two water molecules lie close to the barycentre, as discussed above. The three corresponding Connolly surfaces are represented in Figure 12a), b), and c), respectively. The partial molar volume of the two closely bound water molecules is $V^0(H_2O) = 13 \pm 3\ cm^3 mol^{-1}$. This is lower than the volume of bulk water ($18\ cm^3 mol^{-1}$), and is due to the presence of electrostriction forces around the complex. The value obtained is in good agreement with a semi-empirical prediction of $13.5\ cm^3 mol^{-1}$.[39,40] From these volumes we can calculate the reaction volume of isomerization ($\Delta V^0 = +10 \pm 5\ cm^3 mol^{-1}$). Based on calculations of 100 configurations, which were equally spaced along the simulation, the estimated errors correspond to one standard deviation.

Discussion

Isomers of the binuclear Ln^{III} complexes of OHEC (Ln = Eu, Gd): Binuclear Ln^{III} (Ln = Y, La, Eu, Gd) complexes of OHEC have previously been characterized in the solid state.[17] The X-ray structures showed that the complexes are centrosymmetric, and contain two separated chelate cages. Recently, a second X-ray structure type has been found for the binuclear complexes of Yb^{III} and Lu^{III} ions.[36] In both types, the metal centers are coordinated by four amine nitrogen atoms of the macrocyclic ligand OHEC and by four acetate oxygen atoms. The two types differ only in the hydration number of the lanthanide (q). For the larger, early lanthanides (La, Eu, Gd), the X-ray structure gave coordination number (CN) = 9 and $q = 1$,[17] while for the heavier lanthanides (Yb, Lu), CN = 8 and $q = 0$ were obtained,[36] that is, the complexes are $[Ln_2(ohec)(H_2O)_2]^{2-}$ and $[Ln_2(ohec)]^{2-}$ (named α and β, respectively, see Figure 12). Furthermore, $Na_2[Ln_2(ohec)(H_2O)_2]\cdot 12H_2O$ is centrosymmetric, whereas $Na_2[Ln_2(ohec)]$ does not have a centre of symmetry. It has been shown in the present study on the binuclear complexes of Eu^{III}, Gd^{III} and Tb^{III} ions, as well as in a previous study of Y^{III} ions,[17] that in aqueous solution the two isomeric forms are in equilibrium. A ^1H NMR study conducted on Y^{III} [17] and the Eu^{III} chelates of OHEC pointed out that the two structure types, centrosymmetric and nonsymmetric, respectively, did not change as such in solution. The number of ^1H NMR peaks for the minor β isomer is double the number observed for the α isomer, and can be directly correlated to the loss of symmetry that arises when going from the major α isomer to the minor β isomer. The equilibrium constant for the α to β interconversion of the Eu^{III} complex at 298 K was found by NMR spectroscopy to be 0.42 (see Table 1). The UV/Vis spectrum afforded a similar equilibrium constant and standard reaction enthalpy and entropy. Luminescence results also confirmed the metal coordination number in solution for each isomer (CN = 9 and $q_\alpha = 1$, and CN = 8 and $q_\beta = 0$). Moreover, MD simulations conducted on $[Gd_2(ohec)(H_2O)_2]^{2-}$ and $[Gd_2(ohec)]^{2-}$ showed that these structures did not change during the 1 ns simulations in aqueous media.

The volume change for the reaction $[Eu_2(ohec)(H_2O)_2]^{2-} \rightleftarrows [Eu_2(ohec)]^{2-} + 2H_2O$ was determined by high-pressure UV/Vis ($\Delta V^0 = +5.7\ cm^3 mol^{-1}$) and NMR spectroscopic ($\Delta V^0 = +3.2\ cm^3 mol^{-1}$) studies, and corresponds to a volume variation per metal center of only 2–3 $cm^3 mol^{-1}$. From MD simulations, the volume for the reaction $[Gd_2(ohec)(H_2O)_2]^{2-} \rightleftarrows [Gd_2(ohec)]^{2-} + 2H_2O$ was found to be about $+10\ cm^3 mol^{-1}$. This corresponds to a variation of volume per metal center of $+5\ cm^3 mol^{-1}$, and is in fair agreement with the experimental results. The easiest way to calculate ΔV^0 from the Connolly volumes would be to sum the molecular volume of β, $V^0(\beta)$, with twice the molecular volume of water ($V^0(H_2O) = 18\ cm^3 mol^{-1}$), and then to subtract the molecular volume of α, $V^0(\alpha)$. However, this calculation does not take into account that the water molecules close to the complex are under the influence of electrostriction forces. We therefore calculated $V^0(\beta + 2H_2O)$, where the water molecules are the ones well localized in the middle of the complex and are close to the Gd^{III} centres. Moreover, these two water molecules have residence times significantly longer than the other two water molecules found close to the complex (four water molecules in total for both isomers, i.e., two per metal centre). This approach also enabled us to calculate the partial molar volume of an electrostricted water molecule ($V^0_{el}(H_2O) = {}^1/_2[V^0(\beta + 2H_2O) - V^0(\beta)]$). We determined that $V^0_{el}(H_2O) = 13.0\ cm^3 mol^{-1}$, which corresponds well with the volume of an electrorestricted water molecule in the first coordination sphere of an aqua ion.[39,40]

The dynamics of the two well-localized water molecules are peculiar for the β isomer in solution. These water molecules are linked through hydrogen bonds to acetates that are close to the metal centres, and, therefore, they have especially long residence times (ca. 100 ps). Indeed, these residence times are about four times longer than the $t_{1/2}$ calculated previously for a series of mononuclear polyaminocarboxylate complexes (20–27 ps), and are twice as long as the $t_{1/2}$ determined for a Gd^{III} polyaminophosphonate-based complex, $[Gd(dotp)]^{5-}$ (DOTP = 1,4,7,10-tetrakis(methylenephosphonic acid)-1,4,7,10-tetraazacyclododecane).[41] The residence time determined corresponds to a water-exchange rate of $1\times10^{10}\ s^{-1}$; this is not much higher than the first-shell water-exchange rate for the extremely labile aqua complex of the Gd^{III} ion, $[Gd(H_2O)_8]^{3+}$ ($k_{ex}^{298}=6.82\times10^{8}\ s^{-1}$),[42] or the second-shell water-exchange rate for $[Cr(H_2O)_6]^{3+}$ ($k_{ex}^{298}=7.8\times10^{9}\ s^{-1}$).[43]

The kinetics for the isomerization $\alpha \underset{}{\overset{k_{is}}{\rightleftharpoons}} \beta$ have been found to be slow ($k_{is}^{298}=73.0\ s^{-1}$) relative to the water exchange for the binuclear complex ($k_{is}^{298}=0.40\times10^{6}\ s^{-1}$). The isomerization for DOTA-like complexes that have a similar charge are much faster still, and could not even be measured. The rate is also slow in comparison to that found for the positively charged $[Eu(dotam)(H_2O)]^{3+}$ complex (DOTAM = 1,4,7,10-tetrakis(2-carbamoylethyl)-1,4,7,10-tetraazacyclododecane; $k_{M}^{298}=1700\ s^{-1}$).[44] This may be the result of the important structural changes required for the interconversion. Firstly, the two water–Gd^{III} bonds, which are also stabilized by hydrogen bonds, must be successively broken, and, secondly, the torsion of the macrocyclic skeleton needs to recover a steady state. This rearrangement proceeds through an expansion to reach a transition state with an overall activation volume of $\Delta V_{is}^{\neq}=+7.9\ cm^3\,mol^{-1}$.

Water exchange: The inner-sphere water-exchange rate for the α isomer ($[Gd_2(ohec)(H_2O)_2]^{2-}$, $k_{ex}^{298}=0.40\times10^{6}\ s^{-1}$) is one order of magnitude lower than that found for similar complexes such as $[Gd(dota)(H_2O)]^{-}$.[18] The usual water exchange mechanism for monohydrated Gd^{III} nine-coordinate polyaminocarboxylate complexes is dissociatively activated.[11] This is also the case for $[Gd_2(ohec)(H_2O)_2]^{2-}$, as shown by the positive activation volume $\Delta V^{\neq}=+7.3\ cm^3\,mol^{-1}$, which is comparable to $+10.5\ cm^3\,mol^{-1}$ for $[Gd(dota)(H_2O)]^{-}$. The especially low water-exchange rate is understandable, because in $[Gd_2(ohec)(H_2O)_2]^{2-}$ the coordinated water molecule is confined within the macrocycle, and is, therefore, less accessible to an incoming water molecule in an interchange process. Moreover, the value of the solid angle Ψ, which quantifies the space available in the ligand for the water molecule, and, therefore, the strength of the Gd^{III}–H_2O bond, can also explain the low water-exchange rate. Indeed, the Ψ calculated for $[Gd_2(ohec)(H_2O)_2]^{2-}$ is about 35% larger than that calculated for $[Gd(dota)(H_2O)]^{-}$[45] and $[Gd(egta)(H_2O)]^{2-}$,[37] in which the water exchange is one and two orders of magnitude faster, respectively.

The proposed I_d mechanism implies a positive entropy of activation similar to $[Gd(dota)(H_2O)]$ ($\Delta S^{\neq}=+48.5\ J\,mol^{-1}\,K^{-1}$). However, for $[Gd_2(ohec)(H_2O)_2]^{2-}$ we found an unexpected negative entropy of activation ($-34\ J\,mol^{-1}\,K^{-1}$). This can be explained by a possible reorganization of the ligand conformation. In particular, an incoming bulk water molecule could be facilitated during the interchange step, and hydrogen bonds may be formed between this molecule and the acetate oxygen atoms, as is observed during the MD simulations. The loss of degrees of freedom for such a water molecule is consistent with the negative entropy. Most of the isomerization mechanisms for similar polyaminocarboxylate complexes (e.g., $[Eu(dotam)(H_2O)]^{3+}$) requires that the rearrangement of the complex is slower than the water exchange (the isomerization rate for the $M \rightleftarrows m$ reaction is four times lower than k_{ex} for the DOTAM complexes).[44] In the binuclear complex, the isomerization rate is four orders of magnitude lower than k_{ex}. This is probably as a result of the requirement that both inner-sphere water molecules must depart simultaneously; this is statistically unlikely. The water-exchange mechanism can be considered to be the first step in the isomerization process, and is followed by a rate-determining step that involves strong intramolecular structural modifications and the eviction of the second coordinated water molecule.

Electronic relaxation of the bis-Gd^{III} and mixed Gd^{III}/Y^{III} complexes of OHEC: The relaxation due to Gd–Gd interactions can be disregarded and only the relaxation due to zero-field splitting interactions need to be considered if the paramagnetic Gd^{III} ion is replaced with a diamagnetic Y^{III} ion. Since the ionic radii of the Gd^{III} and Y^{III} ions are very similar (1.053 and 1.019 Å,[46] respectively), the molecular structures and dynamic behaviour of these compounds in aqueous solution should also be very similar. The isomerization constants (K) for both bis-Gd^{III} and mixed Gd^{III}/Y^{III} complexes of OHEC are comparable, and show that the isomerization process is retained. Since the bis-Y^{III} chelate was doped with 10% Gd^{III} ions, 96% of the Gd^{III} ions are found in the heterobinuclear chelate, and the contribution of the homobinuclear Gd^{III} complex can be neglected. The broader EPR peak line widths observed for both isomers of the bis-Gd^{III} complex relative to those of the mixed Gd^{III}/Y^{III} complex of OHEC can clearly be attributed to the proximity of the paramagnetic centers. For both isomers, the 150 to 300 G broadening of the EPR lines at 0.34 T corresponds to an increase in the transverse electronic relaxation rate from 2 to $4.5\times10^{9}\ s^{-1}$. This enhancement is as important as the zero-field splitting contribution, and increases slightly with temperature. This temperature dependence is not expected for pure dipolar interactions described by the rotational correlation time of the complex,[18] and has to be further analyzed. From a qualitative point of view, the significantly faster electronic relaxation of the bis-Gd^{III} complex of OHEC does not favour relaxivity, particularly when macromolecular complexes are designed to have fast water-exchange rates.

Relaxivity: To fit the relaxivity profiles simultaneously with the EPR and ^{17}O NMR data we assumed that the dynamic behaviour of the molecule, that is, its rotation and translation, is mainly isotropic. Nevertheless, the anisotropy of the

complex is revealed through the different values calculated by MD simulations for the rotational correlation times. Table 4 shows that the rotational correlation time in the Gd–Gd direction (z axis) is about 24% longer than in the x and y directions. In the simultaneous fit we introduced two different values for the rotational correlation times of the water hydrogen or oxygen, $\tau_R(H)$ and $\tau_R(O)$, respectively.[32] The ratio $\tau_R(H)/\tau_R(O)$, which was obtained from the simultaneous fit, is equal to 0.81; this is consistent with the value (0.84) calculated by MD simulations. These values are slightly higher than the values obtained for other systems (0.52–0.7).[10,47]

The equations developed by Freed, which are based on spherical complexes, have been used to describe the outer-sphere relaxivity contribution of the relaxivity[34] even if the shape of the complex is oblong. At first glance, it is surprising that the relaxivity of the binuclear Gd^{III} complex of OHEC is lower than the relaxivity of the smaller $[Gd(dota)(H_2O)]^-$ complex (40% lower at 298 K and 30 MHz).[18] Nevertheless, it is understandable when you consider that only $[Gd_2(ohec)(H_2O)_2]^{2-}$, which is present in about 70%, contributes to the inner-sphere relaxivity, r_1^{is}. Furthermore, the outer-sphere relaxivity (r_1^{os}) is also decreased, because the particular shape of the complex limits the bulk water access around both Gd^{III} chelates. We attempted to probe this peculiar behaviour by increasing the distance of closest approach between the free water molecules and the complex a_{GdH} from the usual value of 3.5 Å (e.g., $[Gd(dota)(H_2O)]^-$[18]) to 4.5 Å. This had the effect of decreasing the r_1^{os} value. The fact that the variable temperature relaxivity profiles observed in Figure 10 overlap with each other indicates that relaxivity variation with respect to temperature is not monotonous. This is expected for high-molecular-weight chelates,[1,4,5,7,8] but not for low-molecular-weight ones because relaxivity is normally limited by the rotational correlation time τ_R. Decreases in temperature slow down the tumbling, and this then enhances relaxivity.[11] This uncommon behaviour is not caused by a change in the populations of both isomers versus temperature, but is principally a result of a different temperature behaviour of the outer-sphere contributions for $[Gd_2(ohec)(H_2O)_2]^{2-}$ and $[Gd_2(ohec)]^{2-}$ (Figure 10).

The unfavourable increase in the electronic relaxation rate is not of prime importance for the complex under investigation. However, in the case of macromolecular assemblies that have close Gd^{III} chelates and fast water exchange, such as micelles or dendrimers, the relaxivity would significantly decrease at MRI fields and the electronic relaxation rate would be the limiting factor for such systems.

Conclusion

For the first time we have evidenced and characterized, in detail, an equilibrium between the two coordination sites of a Ln^{III} polyaminocarboxylate complex (CN = 8 and CN = 9) in which only the hydration number of Ln^{III} (i.e., $q = 0$ and $q = 1$, respectively) differs. Such behaviour has never previously been observed for similar mononuclear complexes. In addition to characterizing the two isomers $[Ln_2(ohec)(H_2O)_2]^{2-}$ and $[Ln_2(ohec)]^{2-}$, we clearly proved the existence of an interaction between the two Gd^{III} ions by substituting one paramagnetic Gd^{III} ion with one diamagnetic Y^{III} ion. The Gd–Gd intramolecular electron-spin interaction contributes to the transverse electronic relaxation to a large extent. This has to be taken into account in the design of macromolecular systems of Gd^{III} chelates that have high water-exchange rates, because the electronic relaxation becomes the limiting factor. The design of such systems would enable verification of this assumption. However, treatment of the resulting relaxation data would be particularly difficult outside the Redfield limits.

Experimental Section

Sample preparation: The binuclear Ln^{III} (Ln = Y, Eu, Gd, Tb) chelates were prepared as previously described by mixing one equivalent of the ligand OHEC (octaazacyclohexacosane-1,4,7,10,14,17,20,23-octaacetic acid) with slightly less than two equivalents of Ln^{III} perchlorate. The pH of the mixtures was adjusted to nine, and then they were refluxed until the solutions became clear. The binuclear chelates were crystallized by the slow diffusion of ethanol (99.8%, Merck, p.a.).[15–17]

The solutions for EPR, ^{17}O NMR, and ^1H NMRD measurements were all prepared by dissolving a weighed amount of the complex in doubly-distilled water. The concentration of the Gd^{III} ion was checked by inductively coupled plasma (ICP). The reference (water at pH 9) sample used for the ^{17}O NMR measurements was enriched to 1%, while the solutions of the Gd^{III} chelate were enriched to 2% with 10% ^{17}O-enriched water (Yeda R&D Co., Rehovot, Israel). The solutions used for the ^1H and ^{13}C NMR studies were prepared by dissolving the chelates in 99.5% deuterated water. To avoid mononuclear chelate formation and subsequent release of the free metal ions, known amounts of sodium hydroxide (Merck, p.a.) were used to adjust the pH of all the samples to 8.5–9.[36] The absence of free Ln^{III} ions was checked by the common visual test using eriochrome black T indicator.[48]

NMR measurements: ^1H NMR spectra of the Eu^{III} binuclear complex were recorded at variable temperature and pH using a Bruker Avance-600 (14.1 T, 600 MHz) spectrometer. For all measurements, the temperature was fixed with a gas flow and checked by a substitution method.[49] Variable pressure ^1H NMR measurements were performed up to 200 MPa on a Bruker ARX 400 spectrometer (9.4 T, 400 MHz) equipped with a customized narrow bore high-resolution probehead (5 mm NMR tubes).[50] The temperature was set to 279.4 K by circulating a thermostated liquid through the probe and was measured using a built-in Pt resistor. For these NMR studies, the concentration of the chelate were around 20 mM. The ^1H NMR spectra were calibrated with H_2O (HDO), which was fixed at 4.8 ppm downfield of TMS. The ^1H 1D spectra consisted of 400 scans for the variable temperature study and 2000 scans for the high-pressure NMR study. The signal-to-noise ratio was improved by subtracting an exponential line broadening of 5 Hz in the data analysis.

For all 2D NMR spectra the sweep-width was 60 ppm. Details for ^1H COSY45, ^1H–^{13}C HMQC, ^1H Clean-TOCSY and ^1H EXSY spectra are available in the Supporting Information.

^{17}O NMR data for the binuclear Gd^{III} complex of OHEC were recorded on Bruker ARX-400 (9.4 T, 54.2 MHz) and Bruker AC-200 (4.7 T, 27.1 MHz) spectrometers. Bruker VT 1000 and VT 2000 temperature control units were used to maintain a constant temperature. Transverse and longitudinal ^{17}O relaxation rates and chemical shifts were measured for temperatures between 273 and 340 K. The concentration of the solution was 21.87 mmol kg^{-1}. The samples were sealed in glass spheres adapted for 10 mm NMR tubes to avoid susceptibility corrections of the chemical shifts.[51] High-pressure ^{17}O NMR measurements were performed up to 200 MPa at 312 K with a home-built probehead[50] on a Bruker ARX-400 (9.4 T, 54.2 MHz) spectrometer. The concentration of the solution with respect to the Gd^{III} ion was 45.17 mmol kg^{-1}. The longitudinal and trans-

verse relaxation times, T_1 and T_2, were obtained with the Inversion-Recovery[52] and the Carr–Purcell–Meiboom–Gill[53] spin-echo techniques, respectively.

^{1}H NMRD relaxivity: Increases in the longitudinal ^{1}H relaxation rates of the binuclear Gd^{III} complex of OHEC ($C_{Gd^{III}} = 1.88$ mM) were measured at 278.2, 288.2, 298.2, 310.2 and 323.2 K. The measurements were performed on a Stelar Spinmaster FFC (Fast Field Cycling) relaxometer equipped with a VTC90 temperature control unit (7×10^{-4}–0.47 T, 0.01–20 MHz) and a variable field 1.4 T electromagnet connected to a Bruker Avance-200 console equipped with a home-built tunable probehead (0.47–1.18 T, 20–50.1 MHz) and on a Bruker Avance-200 (4.7 T, 200 MHz) spectrometer. The samples were sealed in cylindrical tubes.

UV/Vis spectroscopy: The absorbance spectra (577.5–581.5 nm) for the binuclear Eu^{III} chelate of OHEC were recorded at variable temperature (275.5–338.5 K, $C_{Eu^{III}}$ about 30 mM) and variable pressure ($C_{Eu^{III}}$ about 10 mM) on a Perkin–Elmer Lambda 19 spectrometer. The measurements were carried out in a thermostatically controlled cell with a 1 cm optical pathlength. The variable pressure measurements were carried out at 298.2 K in a Le Noble 2 cm piston-type cell.[54]

EPR spectroscopy: The X-band spectra (0.34 T, 9.44 GHz) were recorded on a Bruker ESP 300E spectrometer in continuous wave mode for both the binuclear Gd^{III} and the mixed Y^{III}/Gd^{III} chelates of OHEC. The samples were sealed in 1 mm quartz tubes. The mixed Y^{III}/Gd^{III} complex was prepared according to the procedure described above, whereby the binuclear Y^{III} complex of OHEC was doped with a 10% solution of Gd^{III} ions. The Gd^{III} ion concentration of each solution was 40.7 and 5.3 mmol kg^{-1}, respectively.

Luminescence measurements: The experimental procedures for the high-resolution, laser-excited luminescence measurements have been published previously.[55] Solid-state samples were finely powdered and low temperatures (295–10 K) were achieved by means of a Cryodyne Model 22 closed-cycle refrigerator (CTI Cryogenics). The solution studies were carried out at 295 K in water ($C_{Eu^{III}} = 1$ or 0.1 mM) or in D_2O ($C_{Eu^{III}} = 1$ mM) at pH 9. Broad-band excitation ($^5D_2$) of the samples was accomplished by use of the continuous Coherent Innova-90 8 W argon laser at 465.8 nm. Luminescence spectra were corrected for instrumental function, but this was not done for the excitation spectra. Lifetimes quoted are the averages of three independent determinations, and were measured using excitation provided by a Quantum Brillant Nd:YAG laser equipped with a frequency doubler, tripler, and quadrupler, as well as with an OPOTEK *Magic*Prism™ OPO crystal. Lifetimes obtained by selective excitation of the Eu^{III} $^5D_0$ level were measured using a Lambda-Physik-FL3002 pulsed dye laser pumped at 532 nm.

Data analysis: The ^{1}H 1D NMR and EPR spectra were analyzed by fitting Lorentzian functions using the NMRICMA 2.8[56] program for Matlab.[57] The adjustable parameters were: resonance frequency, line width, baseline, intensity and phasing. To extract rate constants from the experimental ^{1}H NMR spectra, a complete line-shape analysis based on the Kubo–Sack formalism was also performed by using NMRICMA 2.8.[22,23,58] The UV/Vis spectra were obtained by fitting the experimental spectra with a convolution Gaussian–Lorentzian by using the Visualiseur/Optimiseur programs on a Matlab platform.[59,60] The least-squares fit for the ^{17}O NMR, electronic and NMRD relaxation data was also performed with this program. The multi-peak fitting of the high-resolution emission spectra was accomplished using Origin 7 and the fitting wizard. The errors for the fitted parameters correspond to one standard deviation.

Computational methods: Classical molecular dynamic simulations on the two different isomers of the binuclear Gd^{III} complex of OHEC were performed in aqueous solution. In the MD-α simulation, the starting structure corresponded to the X-ray crystallographic structure of $[Gd_2(ohec)(H_2O)_2]^{2-}$.[17] The starting structure in the MD-β simulation was isolated from the crystallographic structure of the $[Yb_2(ohec)]^{2-}$ complex.[36] The method of simulation is described elsewhere.[37] Atomic charges were calculated for all the solute atoms at the RHF level by the Mulliken method with the Gaussian 98[61] program with a 6-31G** basis set. Calculations were carried out on Gd^{III} ions, with all 4f electrons frozen, by means of the effective-core potential of Dolg et al.[62] In MD-β, both Yb^{III} ions were replaced by two Gd^{III} ions. The two simulations were performed on a ten node Debian Linux cluster by using the Amber program.[63] The initial structures were placed into a TIP3P water bath with two K^+ counter ions in order to warrant a global neutral electric charge. After a 1000-step energy minimization of the system, a simulation over 25 ps was performed with the frozen complex to equilibrate the water bath. Both the MD-α and MD-β simulations were then carried out for a period of 1 ns at 300 K and 0.1 MPa. Simulation trajectory files were analyzed using a custom program that was run on the Matlab environment. Connolly surfaces and volumes[64] were computed with the Cerius^2 package,[65] with a grid density of 64 points per Å^3, and a probe radius of 1.4 Å.

Acknowledgements

We thank Alain Borel for customizing NMRICMA for this particular system, and for his availability to discuss it with us. We thank Lothar Helm for helpful discussions. We are indebted to Frédéric Gumy for his help in the luminescence measurements. We are grateful to Harry Weisshoff and particularly to Joel Tolman for their support during the recording of the 2D-NMR spectra. We warmly thank Éva Tóth and Paul Salter for reading this manuscript, and Corinne Daguenet for her pertinent remarks during this study. This work is supported by the Swiss National Science Foundation and the Swiss Federal Office for Science and Education, and was performed within the EU COST Action D18.

[1] E. Tóth, L. Helm, A. E. Merbach in *The Chemistry of Contrast Agents in Medical Magnetic Resonance Imaging* (Eds.: A. E. Merbach, E. Tóth), Wiley, Chichester, **2001,** Chapter 2, p. 45.
[2] R. B. Lauffer, D. J. Parmelee, S. U. Dunham, H. S. Ouellet, P. P. Dolan, S. Witte, T. McMurry, R. C. Walovitch, *Radiology* **1998**, *207*, 529.
[3] K. Adzamli, E. Tóth, M. P. Periasamy, S. H. Koenig, A. E. Merbach, M. D. Adams, *MAGMA* **1999**, *8*, 163.
[4] E. Tóth, D. Pubanz, S. Vauthey, L. Helm, A. E. Merbach, *Chem. Eur. J.* **1996**, *2*, 209.
[5] G. M. Nicolle, E. Tóth, H. Schmitt-Willich, B. Radüchel, A. E. Merbach, *Chem. Eur. J.* **2002**, *8*, 1040.
[6] J. P. André, H. R. Maecke, E. Tóth, A. E. Merbach, *J. Biol. Inorg. Chem.* **1999**, *4*, 341.
[7] G. M. Nicolle, E. Tóth, K.-P. Eisenwiener, H. Mäcke, A. E. Merbach, *J. Biol. Inorg. Chem.* **2002**, *7*, 757.
[8] F. A. Dunand, E. Tóth, R. Hollister, A. E. Merbach, *J. Biol. Inorg. Chem.* **2001**, *6*, 247.
[9] R. Ruloff, E. Tóth, R. Scopelliti, R. Tripier, H. Handel, A. E. Merbach, *Chem. Commun.* **2002**, 2630.
[10] S. Laus, R. Ruloff, E. Tóth, A. E. Merbach, *Chem. Eur. J.* **2003**, *9*, 3555.
[11] J. Xu, S. J. Franklin, D. W. Whisenhunt, Jr., K. N. Raymond, *J. Am. Chem. Soc.* **1995**, *117*, 7245.
[12] D. M. J. Doble, M. Botta, J. Wang, S. Aime, A. Barge, K. N. Raymond, *J. Am. Chem. Soc.* **2001**, *123*, 10758.
[13] M. Wagner, R. Ruloff, E. Hoyer, W. Gründer, *Z. Naturforsch. Teil C* **1997**, *52*, 508.
[14] E. Tóth, L. Helm, A. E. Merbach, R. Hedinger, K. Hegetschweiler, A. Jánossy, *Inorg. Chem.* **1998**, *37*, 4104.
[15] H. Schumann, U. Boettger, K. Zietzke, H. Hemling, G. Kociok-Koehn, J. Pickardt, F.-E. Hahn, A. Zschunke, B. Schiefner, H. Gries, B. Raduechel, J. Platzek, *Chem. Ber./Recl.* **1997**, *130*, 267.
[16] H. Schumann, U. Boettger, A. Zschunke, H. Weisshoff, B. Ziemer, *Mater. Sci. Forum* **1999**, *315–317*, 128.
[17] H. Schumann, U. Boettger, H. Weisshoff, B. Ziemer, A. Zschunke, *Eur. J. Inorg. Chem.* **1999**, 1735.
[18] D. H. Powell, O. M. Ni Dhubhghaill, D. Pubanz, Y. Lebedev, W. Schlaepfer, A. E. Merbach, *J. Am. Chem. Soc.* **1996**, *118*, 9333.
[19] J. F. Desreux, *Inorg. Chem.* **1980**, *19*, 1319.
[20] S. Aime, B. Botta, *Inorg. Chim. Acta* **1990**, 101.
[21] S. J. Franklin, K. N. Raymond, *Inorg. Chem.* **1994**, *33*, 5794.
[22] R. Kubo, *J. Phys. Soc. Jpn.* **1954**, *9*, 888.
[23] R. A. Sack, *Mol. Phys.* **1958**, *1*, 163.
[24] N. Graeppi, D. H. Powell, G. Laurenczy, L. Zekany, A. E. Merbach, *Inorg. Chim. Acta* **1995**, *235*, 311.

[25] S. Rast, A. Borel, L. Helm, E. Belorizky, P. H. Fries, A. E. Merbach, *J. Am. Chem. Soc.* **2001**, *123*, 2637.
[26] S. T. Frey, W. D. Horroks, Jr., *Inorg. Chim. Acta* **1995**, 383.
[27] W. D. Horroks, D. R. Sudnick, Jr., *J. Am. Chem. Soc.* **1979**, *101*, 334.
[28] A. Beeby, I. M. Clarkson, R. S. Dickins, S. Faulkner, D. Parker, L. Royle, A. S. de Sousa, J. A. G. Williams, M. Woods, *J. Chem. Soc. Perkin Trans. 2*, **1999**, *3*, 493.
[29] R. M. Supkowski, W. D. Horroks, Jr., *Inorg. Chim. Acta.* **2002**, *340*, 44.
[30] S. Zhang, K. Wu, A. D. Sherry, *Angew. Chem.* **1998**, *110*, 3382; Angew . *Chem. Int. Ed.* **1999**, *38,* 3192.
[31] S. Aime, D. D. Castelli, E. Terreno, *Angew. Chem.* **2002**, *114*, 4510; *Angew. Chem. Int. Ed.* **2002**, *41*, 4334.
[32] F. A. Dunand, A. Borel, A. E. Merbach, *J. Am. Chem. Soc.* **2002**, *124*, 710.
[33] G. Gonzalez, H. D. Powell, V. Tissières, A. E. Merbach, *J. Phys. Chem.* **1994**, *98*, 53.
[34] J. H. Freed, *J. Chem. Phys.* **1978**, *68*, 4034.
[35] S. H. Koenig, R. D. Brown III, *Prog. Nucl. Magn. Reson. Spectrosc.* **1991**, *22*, 487.
[36] U. Boettger, B. O'Sullivan, H. Weisshoff, B. Ziemer, C. Mügge, H. Schumann, unpublished results.
[37] F. Yerly, K. I. Hardcastle, L. Helm, S. Aime, M. Botta, A. E. Merbach, *Chem. Eur. J.* **2002**, *8*, 1031.
[38] R. W. Impey, P. A. Madden, I. R. McDonald, *Mol. Phys.* **1982**, *46*, 513.
[39] T. W. Swaddle, M. K. S. Mak, *Can. J. Chem.* **1983**, *61*, 473.
[40] S. F. Lincoln, A. E. Merbach, *Adv. Inorg. Chem.* **1995**, *42*, 1.
[41] A. Borel, L. Helm, A. E. Merbach, *Chem. Eur. J.* **2001**, *7*, 600.
[42] A. Borel, Y. Yerly, L. Helm, A. E. Merbach, *J. Am. Chem. Soc.* **2002**, *124*, 2042.
[43] A. Bleuzen, F. Foglia, E. Furet, L. Helm, A. E. Merbach, J. Weber, *J. Am. Chem. Soc.* **1996**, *118*, 12777.
[44] F. A. Dunand, S. Aime, A. E. Merbach, *J. Am. Chem. Soc.* **2000**, *122*, 1506.
[45] F. Yerly, A. Borel, L. Helm, A. E. Merbach, *Chem. Eur. J.* **2003**, *9*, 5468.
[46] R. D. Shannon, C. T. Prewitt, *Acta Crystallogr. Sect. B* **1969**, *25*, 925.
[47] F. A. Dunand, A. Borel, L. Helm, *Inorg. Chem. Commun.* **2002**, *5*, 811.
[48] G. Brunisholz, R. Cahen, *Helv. Chim. Acta* **1956**, *39*, 2136.
[49] C. Ammann, P. Meier, A. E. Merbach, *J. Magn. Reson.* **1982**, *46*, 319.
[50] A. Cusanelli, L. Nicula-Dadci, U. Frey, A. E. Merbach, *Inorg. Chem.* **1997**, *36*, 2211.
[51] A. D. Hugi, L. Helm, A. E. Merbach, *Helv. Chim. Acta* **1985**, *68*, 508.
[52] R. L. Vold, J. S. Waugh, M. P. Klein, D. E. Phelps, *J. Chem. Phys.* **1968**, *48*, 3831.
[53] S. Meiboom, D. Gill, *Rev. Sci. Instrum.* **1958**, *29*, 688.
[54] W. J. Le Noble, R. Schlott, *Rev. Sci. Instrum.* **1976**, *54*, 2540.
[55] R. Rodríguez-Cortiñas, F. Avecilla, C. Platas-Iglesias, D. Imbert, J.-C. G. Bünzli, A. de Blas, T. Rodríguez-Blas, *Inorg. Chem.* **2002**, *41*, 5336.
[56] L. Helm, A. Borel, NMRICMA 2.8, Lausanne (Switzerland), **2001**.
[57] Matlab, version 5.3.1, Mathworks, **2000**.
[58] L. W. Reeves, K. N. Shaw, *Can. J. Chem.* **1970**, *48*, 3641.
[59] F. Yerly, VISUALISEUR 2.3.4, Lausanne (Switzerland), **1999**.
[60] F. Yerly, OPTIMISEUR 2.3.4, Lausanne (Switzerland), **1999**.
[61] Gaussian 98 (Revision A.10), M. J. Frisch, G. W. Trucks, H. B. Schlegel, G. E. Scuseria, M. A. Robb, J. R. Cheeseman, V. G. Zakrzewski, J. A. Montgomery, Jr., R. E. Stratmann, J. C. Burant, S. Dapprich, J. M. Millam, A. D. Daniels, K. N. Kudin, M. C. Strain, O. Farkas, J. Tomasi, V. Barone, M. Cossi, R. Cammi, B. Mennucci, C. Pomelli, C. Adamo, S. Clifford, J. Ochterski, G. A. Petersson, P. Y. Ayala, Q. Cui, K. Morokuma, P. Salvador, J. J. Dannenberg, D. K. Malick, A. D. Rabuck, K. Raghavachari, J. B. Foresman, J. Cioslowski, J. V. Ortiz, A. G. Baboul, B. B. Stefanov, G. Liu, A. Liashenko, P. Piskorz, I. Komaromi, R. Gomperts, R. L. Martin, D. J. Fox, T. Keith, M. A. Al-Laham, C. Y. Peng, A. Nanayakkara, M. Challacombe, P. M. W. Gill, B. Johnson, W. Chen, M. W. Wong, J. L. Andres, C. Gonzalez, M. Head-Gordon, E. S. Replogle, J. A. Pople, Gaussian, Inc., Pittsburgh PA, **2001**.
[62] M. Dolg, H. Stoll, A. Savin, H. Preuss, *Theor. Chim. Acta* **1989**, *75*, 173.
[63] D. A. Case, D. A. Pearlman, J. W. Caldwell, T. E. Cheatham, W. S. Ross, C. L. Simmerling, T. A. Darden, K. M. Merz, R. V. Stanton, A. L. Cheng, J. J. Vincent, M. Crowley, V. Tsui, R. J. Radmer, Y. Duan, J. Pitera, I. Massova, G. L. Seibel, U. C. Singh, P. K. Weiner, P. A. Kollman, AMBER 6.0, University of California, San Francisco (USA), **1999**.
[64] M. L. Connolly, *Science* **1983**, *221*, 709.
[65] Cerius2, v. 3.0, Molecular Simulations Inc., Cambridge (UK), **1998**.

Received: April 17, 2003 [F5049]

